Charge-density waves and superconductivity as an alternative to phase separation in the infinite-*U* Hubbard-Holstein model

F. Becca, M. Tarquini, M. Grilli, and C. Di Castro
Dipartimento di Fisica and Istituto Nazionale per la Fisica della Materia, Università La Sapienza, Piazzale Aldo Moro, 00185 Roma, Italy
(Received 5 April 1996)

We investigate the density instabilities present in the infinite-*U* Hubbard-Holstein model both at zero and finite momenta as well as the occurrence of Cooper instabilities with a specific emphasis on the role of long-range Coulomb forces. In carrying out this analysis special attention is devoted to the effects of the strong local *e*-*e* interaction on the *e*-ph coupling and particularly to both the static and dynamic screening processes dressing this coupling. We also clarify under which conditions in strongly correlated electron systems a weak additional interaction, e.g., a phonon-mediated attraction, can give rise to a charge instability. In the presence of long-range Coulomb forces, the frustrated phase separation leads to the formation of incommensurate charge density waves. These instabilities, in turn, lead to strong residual scattering processes between quasiparticles and to superconductivity, thus providing an interesting clue to the interpretation of the physics of the copper oxides. [S0163-1829(96)02137-6]

I. INTRODUCTION

Besides large critical temperatures, the superconducting copper oxides display many anomalous normal-state properties.[1] The understanding of these properties is not only a fascinating theoretical challenge, but would also shed light on the pairing mechanism leading to high-temperature superconductivity.

The anomalous properties of the normal phase have been interpreted along two distinct theoretical lines. The low dimensionality of these highly anisotropic systems and their correlated nature have been proposed to be at the origin of a breakdown of the Fermi liquid (FL). In particular the concept of a Luttinger liquid in two dimension[2] was put forward as a new paradigm for the normal state of copper oxides and it was intensively investigated.[3] However, it was recently shown[4] that the Luttinger liquid is only stable in one dimension. Above one dimension, the Fermi-liquid picture is recovered when the bare electron-electron (*e*-*e*) interaction is nonsingular. This result would support the alternative aptitude, which has been to accept the Landau theory of normal FL's as a suitable starting point. The anomalous properties would then arise as a consequence of singular scattering processes at low energy between the quasiparticles. Along this line magnetic scattering has been considered to be responsible for both the anomalous properties of the normal phase and for the superconducting pairing.[5] It was also proposed that excitonic scattering could give rise to the so-called marginal FL,[6] and provide a pairing mechanism. Singular scattering is also obtained by gauge fields,[7] which arise by implementing the resonating-valence-bond idea in the *t*-*J* model.

The above theoretical lines have more recently been joined by a different scenario suggesting phase separation (PS) as a possible source of anomalous scattering and, therefore, of anomalous normal-state behavior.[8,9] Emery and Kivelson[8] suggested that, although long-range Coulomb (LRC) forces spoil PS as a static thermodynamic phenomenon, the frustrated tendency towards PS may still be important and give rise to large-amplitude collective density fluctuations. Approaching the problem within a coarse-grained model, they suggested that these fluctuations may be responsible for the anomalous behavior of the normal phase and for the superconducting pairing. In a recent work,[9] two of us assessed the relevance of charge instabilities (PS or charge density waves) as a mechanism for anomalous scattering, by determining the dynamical effective scattering interactions among Fermi-liquid quasiparticles close to a charge instability, both in the presence and in the absence of LRC forces. This analysis consisted in a microscopic treatment of the Hubbard-Holstein model in the infinite-*U* limit, finding that, both in the presence and in the absence of LRC forces, the dynamic effective interaction has a singular behavior, strongly affecting the single-particle and the transport scattering time. This scenario is obviously sensible if (i) the considered microscopic model displays PS for some parameter region and (ii) the real copper-oxide systems actually are in the proximity of a charge instability.[10] As far as point (i) is concerned, PS seems to be a rather generic and robust phenomenon in the context of strongly interacting systems.[11] Indeed, after PS was shown to be present in the phase diagram of the *t*-*J* model,[12–14] it was pointed out that PS commonly occurs in models with short-range interaction[15–19,11,20] provided the strong local *e*-*e* repulsion inhibits the stabilizing role of the kinetic energy. Moreover, it was repeatedly claimed that PS and superconductivity can be related phenomena irrespective of the nature of the short-range interaction.[11]

On the other hand, the frequent occurrence of PS in models of strongly interacting electrons is made intriguing by the observation of PS in oxygen-doped superconducting copper oxides (La_2CuO_{4+y}) of the 214 class.[10] Although the electronic origin of PS in these cuprates is still to be established, the contemporary presence of a strong *e*-*e* interaction and of

PS in a real system and the robustness of the PS concept in theoretical models is suggestive. The reason why only La_2CuO_{4+y} seems to phase separate is that LRC forces effectively oppose the separation of charged particles. Only when the negatively charged oxygen ions are sufficiently mobile can the positive holes separate, being accompanied by the oxygen countercharges which compensate for the charge unbalance. Nevertheless, even in those systems where LRC forces are present to prevent a thermodynamic instability, phase separation may remain in the system in the form of a tendency toward charge aggregation, possibly giving rise to superconductivity[8,16–19,11,20] or to anomalous normal properties.[8,9] In particular it might well happen that the long-wavelength density fluctuations associated with PS are suppressed in favor of shorter-wavelength density fluctuations, giving rise either to dynamical slow density modes[8] or to incommensurate charge density waves (CDW's).[21] This latter possibility was recently put forward to explain neutron-scattering results in a $La_{1.48}Nd_{0.4}Sr_{0.12}CuO_4$ sample.[22] In this case it was proposed that the (low-temperature tetragonal) lattice structure and the filling (close to $1+1/8$ holes per CuO_2 cell) were suited to pin the density fluctuations giving rise to a static CDW phase. The formation of striped patterns in the CuO_2 planes of Bi-2212 compounds was also shown from extended x-ray-absorption fine-structure (EXAFS) experiments.[23] Local density fluctuations could also account for some results of neutron scattering experiments in 123 materials.[24,25]

Based on the observation of an antiferromagnetic phase close to the superconducting one in the phase diagram of the copper oxides, previous analyses put emphasis on the role of magnetic coupling in originating the slow density fluctuations.[8] However, the generic occurrence of PS in theoretical models with different interactions indicates that a definite choice of the mechanism leading to PS could be misleading or premature in the absence of more stringent experimental indications. Moreover, while in the models mentioned above the additional interactions inducing PS are of purely electronic origin, it was shown in Ref. 20 that, in the presence of a strong local repulsion, also the lattice may introduce an effective attraction determining PS in the Fermi liquid. This latter result showed within an infinite-U three-band Hubbard model that the instability occurred for reasonable values of the e-ph coupling, indicating that PS by no means requires unlikely parameters, unusual mechanisms, or purely electronic interactions, but it can simply result from the interplay between the strong local repulsion and the (weak) additional attraction provided by the lattice. This theoretical observation is accompanied by some experimental evidence that the lattice can play a non-negligible role in determining the physics of the superconducting cuprates.[26] In particular a sizable coupling between some phonons and the carriers is implied by the presence of polaronic effects[27] for the very lightly doped compounds, by the copper and oxygen isotopic effect present in $La_{2-x}Sr_xCuO_4$, by the Fano line shapes in Raman spectra, and by the rather large frequency shift and linewidth broadening of some phonons at T_c.

In the present paper we pursue the investigation along the route opened in Ref. 20. The occurrence of a phase-separation instability was justifyied within a general Fermi-liquid analysis, demonstrating that the strong interaction is responsible for vertex corrections, which are strongly dependent on the $v_F q/\omega$ ratio, where v_F is the Fermi velocity and q and ω are the transferred momentum and frequency, respectively. These corrections generically lead to a strong suppression of the effective coupling between quasiparticles mediated by (a single) phonon exchange in the $v_F q/\omega \gg 1$ limit. However, such an effect is not present when $v_F q/\omega \ll 1$, which is the relevant limit for the effective interactions entering the Fermi-liquid expression for the compressibility. In these effective interactions in the dynamical limit, the e-ph coupling is therefore not effectively screened, opening the way to a possible violation of the stability criterion for the Fermi liquid in some regions of the parameter space. In Ref. 20 a detailed analysis was then carried out using a slave-boson approach for the infinite-U three-band Hubbard model describing the basic structure of a CuO_2 plane in copper oxides. In the presence of a coupling between the local hole density and a dispersionless optical phonon, it explicitly confirmed the strong dependence of the hole-phonon coupling on the transferred momentum versus frequency ratio and it was also found that the exchange of phonons leads to an unstable phase with negative compressibility already at rather small values of the bare hole-phonon coupling. Close to the unstable region, Cooper instabilities both in s- and d-wave channels were detected, supporting a possible connection between phase separation and superconductivity in strongly correlated systems.

We now start from the infinite-U single-band Hubbard model in the presence of an optical phonon coupled to the local electron density.[28] Due to its relative simplicity with respect to the three-band Hubbard model, *we will be able to extend the model in a rather direct and straigthforward way so as to include the LRC forces between the electrons*. This extension is particularly important since, as mentioned above, LRC forces obviously affect the occurrence of PS instabilities and could provide a clue in explaining the relative rarity of this phenomenon in the real materials. In this way, as briefly reported in Ref. 9, we also provide a microscopic derivation of an incommensurate CDW instability directly from a system of strongly correlated electrons with all the physical implications indicated above. Therefore this topic represents a key issue of our investigation and may definitely be considered as the main point of our analysis.

In Sec. II we introduce the model and the formalism. Readers who are not interested in technical details can directly move to Sec. III, where we present the results concerning the physical properties of the model in the absence of LRC forces. The effects of LRC interactions are reported in Sec. IV, which thus represents the core of the present paper, while in Sec. V we discuss the results and draw our conclusions.

II. HUBBARD-HOLSTEIN MODEL

Our starting point Hamiltonian is the two-dimensional Hubbard model with an additional dispersionless phonon mode A coupled in the manner of Holstein:

$$H=-t\sum_{\langle i,j\rangle,\sigma}(c^{\dagger}_{i\sigma}c_{j\sigma}+\text{H.c.})-t'\sum_{\langle\langle i,j\rangle\rangle,\sigma}(c^{\dagger}_{i\sigma}c_{j\sigma}+\text{H.c.})$$
$$-\mu_0\sum_{i\sigma}n_{i\sigma}+U\sum_i n_{i\uparrow}n_{i\downarrow}+\omega_0\sum_i A^{\dagger}_iA_i$$
$$+g\sum_{i,\sigma}(A^{\dagger}_i+A_i)(n_{i\sigma}-\langle n_{i\sigma}\rangle), \tag{1}$$

where $\langle i,j\rangle$ and $\langle\langle i,j\rangle\rangle$ indicate nearest-neighbor (NN) and next-nearest-neighbor sites, respectively, and $n_{i\sigma}=c^{\dagger}_{i\sigma}c_{i\sigma}$ is the local electron density. Since we are interested in the limit of strong local repulsion, we take the limit $U\to\infty$, which gives rise to the local constraint of no double occupation, $\Sigma_\sigma n_{i\sigma}\leqslant 1$. To implement this constraint we use a standard slave-boson technique[29–33] by performing the usual substitution $c^{\dagger}_{i\sigma}\to c^{\dagger}_{i\sigma}b_i$, $c_{i\sigma}\to b^{\dagger}_i c_{i\sigma}$. We also use a large-$N$ expansion[30] in order to introduce a small parameter, allowing for a systematic perturbative expansion without any assumption on the smallness of any physical quantity. Within the large-N scheme, the spin index runs from 1 to N and the constraint assumes the form $\Sigma_\sigma c^{\dagger}_{i\sigma}c_{i\sigma}+b^{\dagger}_ib_i=N/2$. A suitable rescaling of the hoppings $t\to t/N$ and $t'\to t'/N$ must, in this model, be joined by the similar rescaling of the e-ph coupling $g\to g/\sqrt{N}$ in order to compensate for the presence of N fermionic degrees of freedom. The model can then be represented as a functional integral

$$Z=\int Dc^{\dagger}_{\sigma}Dc_{\sigma}Db^{\dagger}DbD\lambda DADA^{\dagger}\exp\left(-\int_0^{\beta}Sd\tau\right), \tag{2}$$

$$S=\sum_i\left[\sum_\sigma c^{\dagger}_{i\sigma}\frac{\partial c_{i\sigma}}{\partial\tau}+b^{\dagger}_i\frac{\partial b_i}{\partial\tau}+A^{\dagger}_i\frac{\partial A_i}{\partial\tau}\right]$$
$$+\sum_i\left[i\lambda_i\left(b^{\dagger}_ib_i-\frac{N}{2}\right)\right]+H, \tag{3}$$

$$H=\sum_{i,\sigma}c^{\dagger}_{i\sigma}c_{i\sigma}(-\mu_0+i\lambda_i)-\frac{t}{N}\sum_{\langle ij\rangle,\sigma}[c^{\dagger}_{i\sigma}c_{j\sigma}b^{\dagger}_jb_i+\text{c.c.}]$$
$$-\frac{t'}{N}\sum_{\langle\langle ij\rangle\rangle,\sigma}[c^{\dagger}_{i\sigma}c_{j\sigma}b^{\dagger}_jb_i+\text{c.c.}]$$
$$-\frac{g}{\sqrt{N}}\sum_{i,\sigma}(A_i+A^{\dagger}_i)(n_{i\sigma}-\langle n_{i\sigma}\rangle)+\omega_0\sum_i A^{\dagger}_iA_i, \tag{4}$$

where a local Lagrange multiplier field λ_i has been introduced to implement the local constraint.

At the mean-field ($N=\infty$) level, the model of Eqs. (2)–(4) is equivalent to the standard, purely electronic $U=\infty$ Hubbard model without coupling to the phonons, which has been widely considered in the literature.[32] In fact, at the mean-field level no role is played by the phonons because our electron-lattice coupling depends on the difference between the local and the average density and this difference naturally vanishes in the mean-field approximation.[34] The average number of particles per cell is $n=(1-\delta)N/2$ and $\delta=0$ corresponds to half-filling, when one-half electron per cell and per spin flavor is present in the system.

The mean-field self-consistency equations are obtained by requiring the stationarity of the mean-field free energy and they determine the values of $b_0^2\equiv Nr_0^2=\langle b_i\rangle^2$ and of $\lambda_0\equiv i\langle\lambda_i\rangle$. Then the mean-field Hamiltonian reads

$$H_{\text{MF}}=\sum_{k\sigma}E_kc^{\dagger}_{k\sigma}c_{k\sigma}-(\mu_0-\lambda_0)\sum_{k\sigma}c^{\dagger}_{k\sigma}c_{k\sigma}+N\lambda_0\left(r_0^2-\frac{1}{2}\right), \tag{5}$$

where $E_k=-2tr_0^2\varepsilon_k$ is the quasiparticle band with $\varepsilon_k\equiv(\cos k_x+\cos k_y)+\alpha[\cos(k_x+k_y)+\cos(k_x-k_y)]$ (we define $\alpha\equiv t'/t$). In particular it turns out that the square of the mean-field value of the slave-boson field b_0, $b_0^2=Nr_0^2=N\delta/2$, multiplicatively reduces the hopping, $t\to tb_0^2$, thus enhancing the effective mass of the quasiparticles. Moreover, at this level the single-particle self-energy does not introduce a finite quasiparticle lifetime. Then, in this model the single-particle Green function of the physical fermions at $N=2$ has a quasiparticle pole with a finite residue given by the square of the mean-field value of the slave-boson field b_0^2. Thus for any finite doping δ the system is a $T=0$ Fermi liquid.

On the other hand, at half-filling $b_0=\delta=0$ and the system is insulating with a vanishing value of both the quasiparticle bandwidth (i.e., an infinite quasiparticle effective mass m^*) and a vanishing residuum of the polar part in the single-particle Green function.

As far as λ_0 is concerned, this quantity rigidly shifts in a doping-dependent way the bare chemical potential μ_0 and is self-consistently determined by the equation

$$\lambda_0\equiv\lambda_0^0+\alpha\lambda_0^1=2t\sum_k f(E_k)\varepsilon_k$$
$$=2t\sum_k f(E_k)(\beta_k+\alpha\gamma_k), \tag{6}$$

where $f(E)$ is the Fermi function and $\beta_k\equiv\cos k_x+\cos k_y$ and $\gamma_k\equiv\cos(k_x+k_y)+\cos(k_x-k_y)$.

The presence of the coupling with the phonons introduces new physical effects when one considers the fluctuations of the bosonic fields. Since only a particular combination $a=(A^{\dagger}+A)/(2\sqrt{N})$ of the phonon fields A and $A^{\dagger}$ is coupled to the fermions, it is more natural to use the field a and to integrate out the orthogonal combination $\tilde{a}=(A-A^{\dagger})/(2\sqrt{N})$. Then the quadratic action for the boson field a reads

$$H_{\text{phon}}=N\sum_{n,i}\frac{\omega_n^2+\omega_0^2}{\omega_0}a^{\dagger}_ia_i, \tag{7}$$

where we have transformed the imaginary time into Matsubara frequencies. Moreover, it is convenient to work in the radial gauge,[31] the phase of the field $b_i=\sqrt{N}r_i\exp(-i\phi)$ is gauged away, and only the modulus field r_i is kept, while λ_i acquires a time dependence $\lambda_i\to\lambda_i+\partial_\tau\phi_i$. Thus one can define a three-component field $\mathcal{A}^{\mu}=(\delta r,\delta\lambda,a)$ where the time- and space-dependent components are the fluctuating part of the boson fields $r_i=r_0(1+\delta r_i)$, $\lambda_i=-i\lambda_0+\delta\lambda_i$, and a_i.

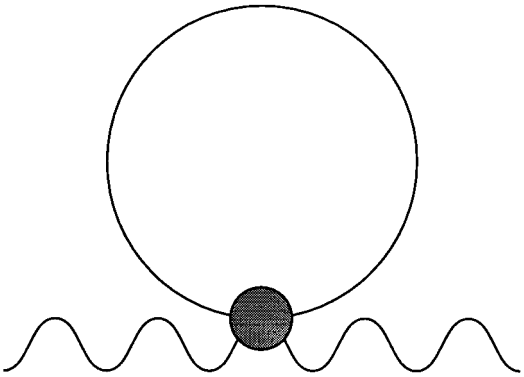

FIG. 1. Leading-order self-energy contribution to the boson propagator from the four-leg vertex in $H_{\rm int}$.

Writing the Hamiltonian of coupled fermions and bosons as $H=H_{\rm MF}+H_{\rm bos}+H_{\rm int}$, where $H_{\rm MF}$ is the above mean-field Hamiltonian, which is quadratic in the fermionic fields, $H_{\rm bos}$ is the purely bosonic part, also including the terms with the a, r, and λ bosons appearing in the action (3) and, in $H_{\rm phon}$, Eq. (7). $H_{\rm int}$ contains the fermion-boson interaction terms. The single-band $U=\infty$ Hubbard model also contains a four-leg vertex arising from the hopping part of the Hamiltonian [see the second term on the (RHS) of Eq. (4)]. The two fermionic legs of this vertex can be contracted (see Fig. 1) giving rise to a leading-order self-energy contribution to the quadratic part of the bosonic Hamiltonian:

$$\Sigma(q)=-2Nr_0^2t\sum_k \varepsilon_{k+q}f(E_k)$$
$$=-\frac{Nr_0^2}{2}[\lambda_0^0\beta_q+\alpha\lambda_0^1\gamma_q]. \tag{8}$$

Fourier transforming to the momentum space, the bosonic part of the action reads

$$H_{\rm bos}=N\sum_{q\mu\nu}\mathcal{A}^\mu(q)B^{\mu\nu}(q)\mathcal{A}^\nu(-q),$$

without explicitly indicating the frequency dependence for the sake of simplicity and where $\mu,\nu=r,\lambda,a$. The matrix $B^{\mu,\nu}$ can be explicitly determined from Eqs. (3)–(8) and it is found that all elements are zero except for $B^{r,r}=r_0^2[\lambda_0^0(1-(1/2)\beta_q)+\alpha\lambda_0^1(1-(1/2)\gamma_q)]$, $B^{r,\lambda}=B^{\lambda,r}=ir_0^2$, and $B^{a,a}=(\omega_n^2+\omega_0^2)/\omega_0$.

The last ingredients of our perturbation theory are the vertices coupling the quasiparticles to the bosons,

$$\Lambda^r(k,q)=-2tr_0^2(\varepsilon_{k+q/2}+\varepsilon_{k-q/2}), \tag{9}$$

$$\Lambda^\lambda(k,q)=i, \tag{10}$$

$$\Lambda^a(k,q)=-2g, \tag{11}$$

allowing us to write the interaction part of the Hamiltonian in the form

$$H_{\rm int}=\sum_{k,q,\sigma} c^\dagger_{k+q/2\sigma}\Lambda^\mu(k,q)c_{k-q/2\sigma}\mathcal{A}^\mu(q). \tag{12}$$

The quasiparticle-boson interactions give rise to self-energy corrections to the boson propagators, which, at leading order in $1/N$, are just fermionic bubbles with insertion of quasiparticle-boson vertices:

$$\Pi^{\mu\nu}(q,\omega_m)=\sum_k \frac{f(E_{k+q/2})-f(E_{k-q/2})}{E_{k+q/2}-E_{k-q/2}-i\omega_m}\Lambda^\mu(k,q)$$
$$\times\Lambda^\nu(k,-q). \tag{13}$$

Once these self-energy corrections are taken into account, the boson propagator at leading order assumes the form

$$D^{\mu\nu}(q,\omega_m)=\langle\mathcal{A}^\mu(q,\omega_m)\mathcal{A}^\nu(-q,-\omega_m)\rangle$$
$$=N^{-1}[2B+\Pi(q,\omega_m)]^{-1}_{\mu\nu}. \tag{14}$$

The factor of 2 multiplying the boson matrix B arises from the fact that the bosonic fields in the presently used radial gauge are real.

The above formal scheme allows us to calculate the leading-order expressions of the effective scattering amplitude both in the particle-hole channel,

$$\Gamma(k,k';q,\omega)=-\sum_{\mu\nu}\Lambda^\mu(k',-q)D^{\mu\nu}(q,\omega)\Lambda^\nu(k,q), \tag{15}$$

and in the particle-particle channel,

$$\Gamma^C(k,k';\omega)=-\sum_{\mu\nu}\Lambda^\mu\left(\frac{k+k'}{2},k'-k\right)D^{\mu\nu}(k-k',\omega)$$
$$\times\Lambda^\nu\left(-\frac{k+k'}{2},k-k'\right). \tag{16}$$

It should be noted that the boson propagators are of order $1/N$ while the occurrence of a bare fermionic bubble leads to a spin summation and is therefore associated with a factor N. Thus, in this $1/N$ approach, the quasiparticle scattering amplitudes are residual interactions of order $1/N$.

The form of the static density-density correlation function at the leading order is

$$P(q,\omega=0)=\frac{1}{N}\sum_{\sigma\sigma'}\langle n_\sigma(q)n_{\sigma'}(-q)\rangle$$
$$=P^0(q,\omega=0)+\sum_{\mu\nu}\chi^0_{n\mu}(q,\omega=0)$$
$$\times D^{\mu\nu}(q,\omega=0)\chi^0_{\nu n}(q,\omega=0), \tag{17}$$

where

$$P^0(q,\omega)=\frac{1}{N}\sum_{\sigma\sigma'}\langle n_\sigma(q)n_{\sigma'}(-q)\rangle_0 \tag{18}$$

is the orbital bare density-density correlation function and

$$\chi^0_{n\mu}(q,\omega)=\frac{1}{N}\sum_{\sigma\sigma'}\left\langle n_\sigma(q)\sum_k c^\dagger_{k\sigma'}\Lambda^\mu(k,q)c_{k+q\sigma'}\right\rangle_0 . \tag{19}$$

A simple inspection of the diagrammatic structure of the scattering amplitudes Γ and of the response functions P, together with the observation that the static fermionic bubbles are nonsingular functions of q, allows us to conclude that both quantities provide the same amount of information as far as the occurrence of the instabilities is concerned. In fact one can immediately recognize that, since a diverging response function can only arise from a diverging boson propagator, also the scattering amplitude mediated by the same boson propagator would diverge at the same time. The same holds for the static Cooper scattering amplitude in the particle-particle channel, which, within our leading-order $1/N$ expansion, coincides with the particle-hole amplitude.[35]

III. PHYSICAL PROPERTIES OF THE HUBBARD-HOLSTEIN MODEL

A. Static properties

The model introduced in the previous section is characterized by the contemporary presence of a very strong local interaction and a phonon-mediated attraction. The main point to be addressed here is the subtle interplay between the attractive and repulsive forces so as to clarify the origin of the effective interactions arising between the quasiparticles giving rise to instabilities for some values of the parameters. We will first analyze the static properties, so that we first focus on the $\omega=0$ limit of the effective interaction in the particle-hole channel, Eq. (15), between quasiparticles on the Fermi surface ($k=k_F$, $k'=k'_F$).

Since in general this quantity involves the calculation of the fermionic bubbles, Eq. (13), entering the expression of the boson propagator, Eq. (14), an explicit analytic evaluation of this scattering amplitude at finite momentum is not possible. The finite momentum analysis of the static scattering amplitude is then carried out numerically. However, we find it instructive to present first the analytic results, which can be obtained in the small transferred momentum limit ($q\to 0$):

$$\begin{aligned}\Gamma_q&=\lim_{q\to 0}\lim_{\omega\to 0}\Gamma(k_F,k'_F;q,\omega)\\&=-\frac{1}{N}\begin{pmatrix}2E_F\\ i\\ -2g\end{pmatrix}\\&\quad\times\begin{pmatrix}\Pi^{rr}_q & i2r_0^2+\Pi^{r\lambda}_q & \Pi^{ra}_q\\ i2r_0^2+\Pi^{r\lambda}_q & \Pi^{\lambda\lambda}_q & \Pi^{\lambda a}_q\\ \Pi^{ar}_q & \Pi^{a\lambda}_q & 2\omega_0+\Pi^{aa}_q\end{pmatrix}^{-1}\\&\quad\times\begin{pmatrix}2E_F\\ i\\ -2g\end{pmatrix},\end{aligned} \tag{20}$$

where the static $q\to 0$ limit of the bubbles, $\Pi^{\mu\nu}_q\equiv\Pi^{\mu\nu}(q\to 0,\ \omega_m=0)$ can easily be evaluated by noticing that at $T=0$

$$\Pi^{\mu\nu}(q\to 0,\ \omega_m=0)=\sum_k\frac{\partial f(E_k)}{\partial E_k}\Lambda^\mu(k,0)\Lambda^\nu(k,0) \tag{21}$$

$$=-\sum_k\delta(E_k-E_F)\Lambda^\mu(k,0)\Lambda^\nu(k,0)$$

$$=-\nu^*\Lambda^\mu(k_F,0)\Lambda^\nu(k_F,0), \tag{22}$$

where ν^* is the quasiparticle density of states at the Fermi level. In the last equality we use the property that the vertices are constant over the Fermi surface. Once the expressions for the bubbles are substituted in Eq. (20) one obtains the final expression for the static scattering amplitude between the quasiparticles:

$$N\nu^*\Gamma_q=\frac{N\nu^*\Gamma_\omega}{1+N\nu^*\Gamma_\omega}=\frac{4t\nu^*\varepsilon_{k_F}-\lambda_g}{1+(4t\nu^*\varepsilon_{k_F}-\lambda_g)}, \tag{23}$$

where we introduced the effective phonon-mediated e-e coupling $\lambda_g\equiv 2\nu^*g^2/\omega_0$. In Eq. (23) the dynamical effective scattering amplitude between the quasiparticles, $\Gamma_\omega=\Gamma(k_F,k_F;\ q=0,\ \omega\to 0)$, is identified by

$$\Gamma_\omega=\frac{1}{N}\left(4t\varepsilon_{k_F}-\frac{\lambda_g}{\nu^*}\right). \tag{24}$$

This latter quantity represents the residual interaction between the quasiparticles on the Fermi surface when their mutual screening is not taken into account. This screening effect is instead included in Γ_q.[36] The above expression for Γ_ω can also be easily obtained from the direct evaluation of Eq. (20) by noticing that in the dynamical limit the fermionic bubbles vanish identically. Thus, using $\Pi^{\mu\nu}=0$ in Eq. (14) one again finds $N\nu^*\Gamma_\omega=4t\nu^*\varepsilon_{k_F}-\lambda_g$.

At this point one recognizes that an instability can in principle take place when the Landau-Pomeranchuk criterion for the stability of a Fermi liquid, $F_0^s\equiv N\nu^*\Gamma_\omega>-1$, is violated, leading to a negatively diverging total (static) scattering amplitude Γ_q:

$$F_0^s=N\nu^*\Gamma_\omega=4t\nu^*\varepsilon_{k_F}-\lambda_g\leqslant -1. \tag{25}$$

As a consequence a divergent compressibility is found,

$$\kappa\equiv\frac{\partial n}{\partial\mu}=\nu^*(1-\nu^*\Gamma_q)=\frac{N\nu^*}{1+F_0^s}\to_{F_0^s\to -1}\infty, \tag{26}$$

which signals the occurrence of a PS. It is worth noting that the phonon parameters only enter the condition for PS via the combination $\lambda_g=2\nu^*g^2/\omega_0$. This implies that, for a given electronic band structure, i.e., for a given ν^*, the *static* instability is obtained for any phonon frequency provided g is suitably rescaled to keep the λ_g fixed (of course too large e-ph couplings put in jeopardy our weak coupling approach, where vertex corrections beyond the Migdal theorem are not included).

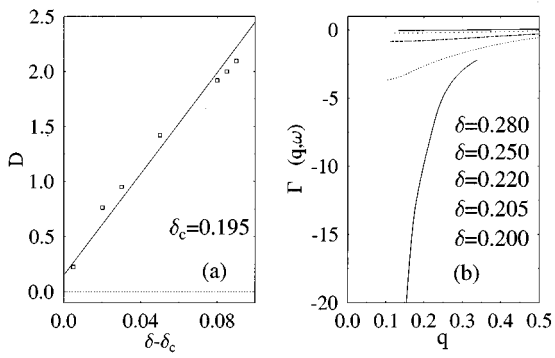

FIG. 2. (a) Doping dependence of the mass D [cf. Eq. (33) below] in the static effective scattering amplitude close to the PS instability. The open squares in (a) indicate the values of D at various dopings and $g_{\rm phys}=g_{c\,\rm phys}=0.194/\sqrt{2}$ eV, $t_{\rm phys}=0.5$ eV, $t'=-(1/6)t$, and $\omega_{0\,\rm phys}=0.04$ eV. For these parameters $\delta_c=0.195$. The solid line is a linear fit. (b) Static scattering amplitude for the same parameters as in (a) as a function of the transferred momentum $\mathbf{q}$ in the (1,0) direction. The doping $\delta=0.2$, 0.205, 0.22, 0.25, and 0.28 increases from the lower solid line to the upper solid line.

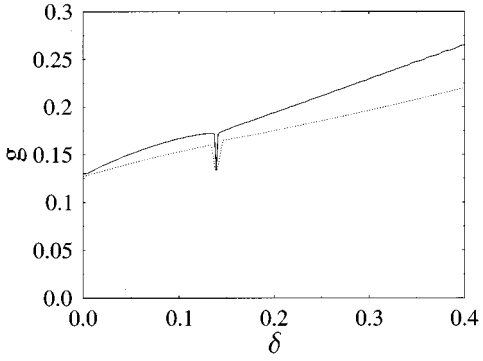

FIG. 3. Phase diagram e-ph coupling g vs doping δ $t_{\rm phys}=0.5$ eV, $t'=-(1/6)t$, and $\omega_{0\,\rm phys}=0.04$ eV. On the solid line the compressibility diverges, whereas the dotted line arises from the Maxwell construction.

It is worth remarking that the quantity $\varepsilon_{k_F}=(\cos k_{xF}+\cos k_{yF})+2\alpha(\cos k_{xF}\cos k_{yF})$ is rather small at low doping.[37] We carried out a detailed investigation of ε_{k_F} as a function of the doping and of the hopping ratio α determining the most appropriate values of t' in order to reproduce within our single-band model Fermi surface shapes in reasonable agreement with those observed in some superconducting copper oxides. According to previous analyses,[38] we found that the values of t' giving rise to reasonably shaped Fermi surfaces for 214 compounds are negative with $t'\simeq-0.167t$. $t'\simeq-0.45t$ was instead adopted to reproduce Fermi surfaces in agreement with those observed in 123 and 2212 compounds. For these values of t', ε_{k_F} remains rather small in the low-doping regime. Therefore, although a minumum critical value g_c of the e-ph coupling is needed for the phase-separation instability to occur, its value can be small and it does not really provide a difficult condition to be satisfied in the real systems.[39]

The main point to be stressed here is that, despite the infinite bare repulsion between the bare particles, a huge screening takes place in the system, introducing attractive forces almost exactly balancing the repulsion and giving rise to a finite scattering amplitude Γ_ω between the quasiparticles. This residual effective interaction is repulsive in the absence of the e-ph coupling, whereas it may turn into an attraction when λ_g is large enough. In this situation, which arises from the strongly interacting nature of the system, even this additional attraction can drive the system to be unstable. This finding matches well previous results obtained in different models and it emphasizes the general robustness of the PS concept in the context of strongly interacting systems. Moreover, this finding supports the choice of the Hubbard-Holstein model as a simple paradigm to describe the physics of PS in the context of strongly interacting systems.

In principle the above analysis cannot exclude that an instability at a finite momentum can take place before PS, thus calling for a more general investigation. This latter has been carried out numerically through the explicit calculation of both the static scattering amplitude at finite transferred momentum and the density-density response function. In Fig. 2 we report the full static scattering amplitude in the particle-particle channel. We choose this quantity because it will also enter the calculation of the Cooper instability reported below. We performed the calculation for various different values of the doping at a value of g larger than the minimum value required to have a PS instability. Here and throughout this paper we express the various quantities in physical units translated from the $1/N$ formalism with $N=2$: $t_{\rm phys}=t/N$, $t'_{\rm phys}=t'/N$, $g_{\rm phys}=g/\sqrt{N}$, and $\omega_{0\rm phys}=\omega_0$.

From the reported results it is natural to conclude that the divergent particle-particle scattering amplitude (i.e., a divergent boson propagator and a consequently diverging density-density response function) occurs at a zero momentum transfer. According to Eq. (26) this divergence ($\Gamma_q\to-\infty$) leads to a diverging compressibility, signaling a PS instability.

As can be seen in the g vs δ phase diagram of Fig. 3, for the $t'=-0.167t$ case (a similar diagram is obtained when $t'=-0.45t$), we found that this behavior is rather generic at low and intermediate doping (solid line).[40] The instability line drawn in the phase diagram indicates where the static density-density response of the system becomes singular. A narrow dip in the instability solid line is due to the presence of a van Hove singularity enhancing ν^*, thus favoring the instability. However, the system becomes unstable and phase separates before the solid line is reached, where $\kappa\to\infty$. A Maxwell construction (dotted line) is needed to determine the region where PS starts. The Appendix briefly describes the procedure to carry out the Maxwell construction.

We complete the static analysis of the model by investigating the possibility of Cooper pairing. As already pointed

TABLE I. Extended s- and d-wave superconducting couplings for $t_{\rm phys}=0.5$ eV, $t=-1/6t'$, $g_{\rm phys}=0.192/\sqrt{2}$ eV, and $\omega_{0\rm phys}=0.04$ eV at various dopings. The instability is at $\delta_c=0.193$.

δ	0.194	0.200	0.205	0.210	0.225
λ_{s_1}	0.458	−0.065			
λ_{d_1}	1.284	0.137	0.092	0.076	0.052

out, in various models with strong e-e correlations superconductivity can appear in the proximity of a PS instability. This can easily be understood by looking at the large attraction arising in the particle-particle effective scattering amplitude close to the instabilities (see Fig. 2). According to this simple observation and according to the previous experience in other strongly interacting models, we therefore investigated the Fermi surface average of the particle-particle scattering amplitude defined in Eq. (16):

$$\lambda_l = -\left[\int dk\,\delta(E_k-\mu)g_l(k)^2\right]^{-1}\int\int dk dk' \times[g_l(k)\Gamma^C(k,k';\omega=0)g_l(k')\,\delta(E_k-\mu)\,\delta(E_{k'}-\mu)], \tag{27}$$

with $g_{s_1}(k)=\cos(k_x)+\cos(k_y)$ and $g_{d_1}(k)=\cos(k_x)-\cos(k_y)$ projecting the interaction onto the s-wave and d-wave channels. (Notice that $\lambda_l>0$ means attraction.)

The results are tabulated at various doping concentrations for the case with $t_{\rm phys}=0.5$ eV, $t=-1/6t'$, $g_{\rm phys}=0.192/\sqrt{2}$ eV, and $\omega_{0\rm phys}=0.04$ eV in Table I. With the set of parameters of Table I the critical doping for the occurrence of the instability is $\delta_c=0.192$. Whereas the couplings λ_d are found to be generally attractive near (and inside) the unstable region, s-wave Cooper instabilities are found only very close to the instability line.[41]

At first sight it may seem strange to investigate and to look for superconductivity in a phase-diagram region, which is made unaccessible by the Maxwell construction. However, one should remember that the phase diagram of Fig. 3 may be modified by several effects. First of all long-range Coulombic forces will spoil PS. This issue is the main topic of the present paper and will be discussed in Sec. IV. Second, temperature effects could restore the uniformity of the system. This issue cannot be reliably addressed within a slave-boson formalism and is beyond the scope of our work. Most importantly superconductivity itself can give rise to a more stable phase competing with and stabilizing PS. In this latter scenario a complex interplay between the PS instability and superconductivity will likely arise: The incipient instability originates superconductivity, which, in turn, prevents the instability to occur.[42] To substantiate these ideas a consistent analysis would be required of the feedback effects, which, however, only appear at higher order in the 1/N expansion. Work in this direction is in progress.

B. Dynamical properties

The analysis carried out in the previous sections was purely static. From this analysis it turned out that the subtle balancing between repulsive forces and attractive screening processes may have relevant physical effects. In this regard a dynamical investigation immediately appears to be of great interest in order to fully clarify the way the various screening effects contribute to the physics of the system.

From the standard Fermi-liquid theory,[36] one obtains the two relations connecting the density vertex $\Lambda^e(q,\omega)$ and the wave function renormalization z^e in the dynamic and static limits:

$$z^e\Lambda^e(q=0,\omega\to 0)=1, \tag{28}$$

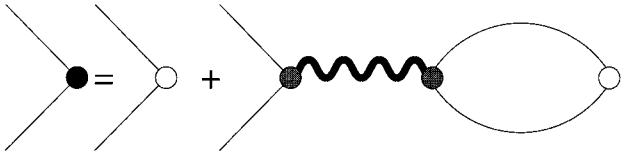

FIG. 4. Leading order in the $1/N$ diagrammatic structure of the effective e-ph vertex dressed by electronic processes only: The wavy line is the slave-boson propagator only involving r and λ bosons, the solid circle is the dressed e-ph vertex, the open circle is the bare e-ph vertex, and the grey circles are the quasiparticle–slave-boson vertices.

$$z^e\Lambda^e(q\to 0,\omega=0)=\frac{1}{1+F_0^{s(e)}}, \tag{29}$$

where $F_0^{s(e)}=2\nu^*\Gamma_\omega^e$ and Γ_ω^e are the Landau parameter and the dynamic ($q=0$, $\omega\to 0$) effective e-e scattering amplitude between the quasiparticles, respectively, when only the e-e repulsion is taken into account. To explicitly keep memory of this limitation we append a suffix e to Γ_ω and to any quantity not involving phononic processes.

In our specific model and within our leading-order $1/N$ approximation one can recognize that the static and dynamical e-ph vertices Λ_q and Λ_ω are related by

$$\Lambda_q^e=\frac{\Lambda_\omega^e}{1+N\nu^*\Gamma_\omega^e}, \tag{30}$$

where Γ_ω^e is the first term in the RHS of Eq. (24) and $\Lambda_\omega^e=1$. Equation (30) shows the difference between the dynamic and static limits, which can be substantial for large ν^*. This is a generic feature of strongly correlated systems, which one has to take into account since it can strongly affect the relevance of the e-ph coupling.

The above small-q and small-ω analysis can easily be extended to finite momenta and frequencies by an explicit numerical evaluation of the diagrams of Fig. 4. In these diagrams one considers the effects of the δr_i and $\delta\lambda_i$ boson fluctuations, keeping track at leading order in $1/N$ of the original infinite Hubbard repulsion U. More explicitly one has to evaluate

$$\Lambda^{e-\rm ph}(k,q;\omega_m)=\Lambda^a(k,q)-N\sum_{\mu,\nu=r,\lambda}\Lambda^\mu(k,q)D^{\mu,\nu}(q,\omega_m)\times\Pi^{\nu,a}(q,\omega_m). \tag{31}$$

For $\omega_m=0$ our slave-boson result is in perfect quantitative agreement with the static analysis carried out in Refs. 43–45 for the single-band infinite-U Hubbard model treated within a large-N expansion by means of Hubbard projectors.

The results of a dynamical analysis of the e-ph vertex vs transferred Matsubara frequencies are reported in Figs. 5(a) and 5(b) for $t'=-t/6$ for a small [$\boldsymbol{q}=(0.2,0)$] and a sizable [$\boldsymbol{q}=(2.0,0)$] value of the transferred momentum, respectively. Similar results are obtained for the $t'=-0.45t$ case. It is worth noting in Fig. 5(a) how rapidly the effective e-ph vertex increases as soon as the transferred frequency becomes larger than some screening scale $\omega_{\rm scr}$ of the order of v_F^*q, with $v_F^*\propto\delta$. A much larger scale of the order of the bare bandwidth t is involved in the slower increase of the

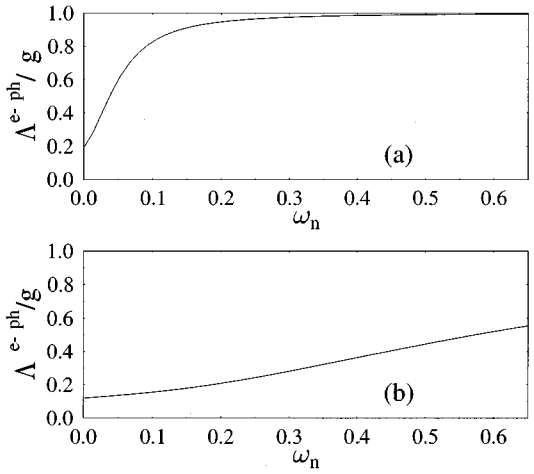

FIG. 5. Effective e-ph vertex as a function of the transferred Matsubara frequency for $t_{\rm phys}=0.5$ eV, $t'=-(1/6)t$, $\omega_{0\,\rm phys}=0.04$ eV, and $\delta=0.205$. In (a) the transferred momentum is small, $\boldsymbol{q}=(0.2,0)$, and it is large, $\boldsymbol{q}=(2.0,0)$, in (b).

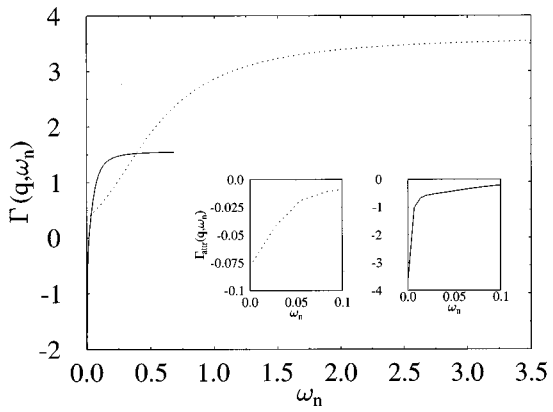

FIG. 6. Effective scattering amplitude as a function of the transferred Matsubara frequency for $t_{\rm phys}=0.5$ eV, $t'=-(1/6)t$, $g_{\rm phys}=0.194/\sqrt{2}$ eV, $\omega_{0\,\rm phys}=0.04$ eV, and $\delta=0.205$. Solid line, small transferred momentum $\boldsymbol{q}=(0.15,0)$; dashed line, large transferred momentum $\boldsymbol{q}=(1.75,0)$. In the insets the attractive parts $\Gamma_{\rm attr}=\Gamma-\Gamma_{\rm rep}$ (see text) are reported for both small (solid line) and large momenta (dashed line).

vertex at large momenta [Fig. 5(b)]. A detailed discussion of the screening scales is deferred to the next section, where this analysis will also be carried out in the presence of LRC forces. Since dynamical effects strongly modify the behavior of the e-ph interaction, it seems natural to extend the dynamical analysis to other relevant quantities of the system. In particular we investigated the finite-frequency behavior of the effective Cooper scattering amplitudes between the quasiparticles on the Fermi surface $\Gamma^C(k_F,k_F\prime,\omega_n)$. The results are reported in Fig. 6 for the particle-particle scattering amplitudes as a function of the transferred Matsubara frequencies both for small and large momenta. In this case the bare e-ph coupling $g_{\rm phys}=0.194/\sqrt{2}$ eV and the doping $\delta=0.205$ are tuned in order to place the system in the proximity of a $q=0$ instability occurring for $g_{c\rm phys}=0.194/\sqrt{2}$ and $\delta_c=0.195$. For clarity we also represent in the inset the difference between the total and the purely repulsive (i.e., involving the r and λ bosons only) part of the scattering amplitude. For any momentum, this attractive part of the interaction lives on a frequency range of the order of the phononic energy. However, as expected, the large and the small-momentum behaviors are strikingly different. At small momenta the attraction mediated by the phonons is stronger because the e-ph coupling is larger (cf. Fig. 5) and, close to the instability, it gives rise to a large attraction at low frequencies. This attraction is the vestige of the huge static attraction found close to the PS instability also in the particle-particle channel (cf. Fig. 2). On the other hand the attractive contribution in the large-momentum case (dotted curve in the inset of Fig. 6) is quite small for any frequency, because the effective coupling between the quasiparticles and the phonons is greatly reduced by the large-momentum screening [cf. Fig. 5(b)].

We finally would like to comment on the behavior of the scattering amplitude for frequencies that are larger than both the phononic and electronic energy scales. In this case it can be easily checked that the fermionic polarization bubbles vanish as ω_n^{-2}, thereby leading to a scattering amplitude determined by the bare slave-boson propagators [the bare phonon propagator $(B^{a,a})^{-1}$ also vanishes for large frequencies]. A simple calculation based on Eq. (16) and on Eq. (14) with $\Pi(q,\omega)\to 0$ gives the large-ω saturation value of the scattering amplitude in the Cooper channel:

$$\Gamma^C(k_F,k_F\prime;\omega\to\infty)=\frac{1}{N}\left[4t\varepsilon_{k_F}+\frac{\lambda_0^0(1-\frac{1}{2}\beta_q)+\alpha\lambda_0^1(1-\frac{1}{2}\gamma_q)}{2r_0^2}\right], \tag{32}$$

where $\lambda_0^{0,1}$ are defined in Eq. (6) and β_q and γ_q are given after Eq. (6). A direct inspection of Fig. 6 shows that this saturation value is reached more rapidly in the small momentum transfer case, whereas a slower rise of $\Gamma^C(\omega)$ is found in the large momentum transfer case of Fig. 6. This result is a natural consequence of the disappearance of the phonons from the high-frequency processes at $(\omega_n>\omega_0)$. Then only electronic processes determine the scattering like in the screening of the e-ph vertex described above [cf. Figs. 5(a) and 5(b)]. Again two energy scales appear to be relevant: a small $\omega_{\rm scr}\sim\delta q$ at small momenta and a large $\omega_{\rm scr}\sim t$ at large momenta. These two scales set the frequency region above which the scattering tends to saturate.

As far as the dynamic behavior of the scattering amplitude in the proximity of a PS instability, we also like, for completeness sake, to recall that a recent work[9] also showed that, close to a $q=0$ instability, the effective dynamical scattering amplitude for real frequencies has a strongly singular behavior. In particular the effective interaction assumes the form

$$\Gamma(q,\omega)\approx\tilde{U}-\frac{1}{Bq^2-i\omega C/q+D}, \tag{33}$$

similar to the one obtained within the gauge-theory treatment of the t-J model,[7] with a mass $D\propto(\delta-\delta_c)$, which vanishes linearly when, by varying the doping, one approaches the $q=0$ instability line. $\tilde{U}$ represents the almost-momentum-independent repulsive contribution to Γ mediated by the r and λ bosons. According to the spirit of the Fermi-liquid

theory, it may be interpreted as the residual repulsion surviving between the quasiparticles and arising from the infinite repulsion U between the bare electrons. Equation (33) establishes a connection between the presence of a $q=0$ charge instability and singular scattering, which could determine the anomalous normal-state properties of the copper oxides.

The analysis summarized in Figs. 5 and 6 is of obvious pertinence in a complete Eliashberg treatment of the superconductivity problem. In particular it is evident that the huge enhancement of the attractive part of the scattering amplitude near the instability line can be responsible for large critical temperatures despite the small e-ph coupling.

The closeness to a phase-separation instability appears therefore as a favorable condition in order to obtain high-temperature superconductivity from a phonon-mediated attraction similarly to what suggested in the context of purely electronic pairing mechanisms.[17]

IV. EFFECT OF LONG-RANGE INTERACTIONS

A. Formal extension

Although we expect the effect of LRC forces to be most effective in the small transferred momentum case, where the underlying lattice structure is less visible, we explicitly kept into account the real symmetry of the square-lattice system. Therefore, to derive an explicit expression for the Coulombic potential in the spirit of the point-charge approximation we started from the discretized form of the Laplace equation. Moreover, since we assume that our two-dimensional model represents planes of a truely three-dimensional lattice we also include a third spatial dimension. For clarity in this section we restore the explicit dependence of the lattice spacing a, which in the previous sections was set to unity in the square two-dimensional lattice. In the third space direction, instead, we assume the unit cell to have a lattice spacing d (i.e., we assume a tetragonal three-dimensional lattice). In this scheme, the Laplace equation reads

$$\epsilon_{\parallel}\sum_{\eta=x,y}\left(\frac{\phi_{i-j+\eta}+\phi_{i-j-\eta}-2\phi_{i-j}}{a^2}\right) \tag{34}$$

$$+\epsilon_{\perp}\left(\frac{\phi_{i-j+z}+\phi_{i-j-z}-2\phi_{i-j}}{d^2}\right)=-e\,\delta(i-j), \tag{35}$$

where i,j are lattice sites and $\epsilon_{\perp}$ and $\epsilon_{\parallel}$ are the dynamic dielectric constants perpendicularly and along the planes, respectively. Fourier transforming one can easily obtain

$$\left[\frac{\tilde{\epsilon}}{(a/d)^2}[\cos(aq_x)+\cos(aq_y)-2]+\cos(dq_z)-1\right]\frac{2\epsilon_{\perp}}{d^2}\phi_{\mathbf{q}} =-e, \tag{36}$$

with $\tilde{\epsilon}\equiv\epsilon_{\parallel}/\epsilon_{\perp}$, from which one gets the expression of the LRC potential in the three-dimensional momentum space:

$$\phi_{\mathbf{q}}=-\frac{ed^2}{2\epsilon_{\perp}}[A(q_x,q_y)+\cos(q_zd)]^{-1}, \tag{37}$$

where we defined

$$A(q_x,q_y)=\frac{\tilde{\epsilon}}{(a/d)^2}[\cos(aq_x)+\cos(aq_y)-2]-1\,. \tag{38}$$

Since we are interested in the effects of the Coulomb potential on the square-lattice planar system, we now transform from q_z to real space for the plane at $z=0$, obtaining

$$\phi_{\mathbf{q}_{\parallel}}(z=0)=-\frac{ed}{2\epsilon_{\perp}}\frac{1}{\sqrt{A^2(q_x,q_y)-1}}. \tag{39}$$

Notice that this is the potential between electrons in a two-dimensional lattice embedded in a three-dimensional space and it diverges as q^{-1} for small transferred momenta, rather than q^{-2} as happens for three-dimensional electronic systems. This potential can be used in the Coulombic part of the Hamiltonian

$$H_C=\frac{V_C}{2N}\sum_q\frac{1}{\sqrt{A^2(q)-1}}\rho_q\rho_{-q}, \tag{40}$$

where $\rho_q\equiv\Sigma_{k,\sigma}c^{\dagger}_{k+q,\sigma}c_{k,\sigma}$ and the Coulombic coupling constant $V_C\equiv e^2d/(2\epsilon_{\perp}a^2)$. It should be noted that, as is customarily done, the sum does not include the zero-momentum component, since we are supposing that the diverging $q=0$ interaction between the electrons is canceled by the contribution of a uniform positively charged ionic background. Having in mind the superconducting copper oxides of the 214 type, where $d\approx 3a$, $t_{\rm phys}\approx 0.5$ eV, $\epsilon_{\parallel}\approx 30$, and $\epsilon_{\perp}\approx 5$ one sees that V_C has to range from roughly 0.5–3 eV in order to have holes in neighboring CuO_2 cells repelling each other with a strength of 0.1–0.6 eV.

The Hamiltonian (40) can then be added to the Hamiltonian of the Hubbard-Holstein model (4) and the product of four fermionic fields can be decoupled by means of a standard Hubbard-Stratonovich transformation. In this way one introduces a new real bosonic field Y_i to be integrated over in the functional integral. Although this spatially fluctuating field does not have its own dynamics, it acquires a frequency dependence via its coupling to the fermionic degrees of freedom. In particular, extending the bosonic space $A^{\mu}(q)=(\delta r_q,\delta\lambda_q,a_q,Y_q)$ (we dropped for simplicity the Matsubara frequency dependence of the bosonic fields) one can extend the formalism of Sec. II to include the effects of the Coulomb potential represented by the Y boson. A direct calculation shows that the quasiparticle-boson vertex is

$$\Lambda^{Y}(k,q)=i, \tag{41}$$

as expected since the Coulomb potential couples to the local electronic density in the same way as the boson λ does. The bare boson propagator becomes a 4×4 matrix with an additional nonzero element:

$$B^{Y,Y}=\frac{\sqrt{A^2(q)-1}}{2V_C}. \tag{42}$$

We stress again that the Y boson does not have any uniform $q=0$ component, which was discarded from the beginning in the sum of Eq. (40) and therefore it does not affect the mean-field results.

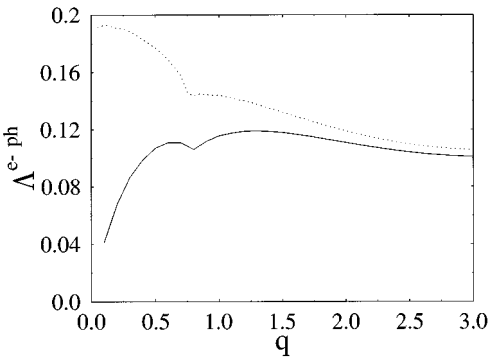

FIG. 7. Static effective e-ph vertex (in units of g_{phys}) as a function of the transferred momentum in the (1,0) direction for $t_{\text{phys}}=0.5$ eV, $t'=-(1/6)t$, and $\omega_{0\,\text{phys}}=0.04$ eV. The dotted line is in the absence of LRC forces ($V_{C\text{phys}}=0$); the solid line is in the presence of LRC forces with $V_{C\text{phys}}=0.55$ eV.

B. Static properties

The introduction of a LRC potential greatly affects the coupling between phonons and electrons particularly for small momenta, where the Coulombic forces are most effective. In fact, since in the Hubbard-Holstein model phonons couple to the local electron densities like the Coulombic potential, the e-ph coupling is effectively screened by particle-hole pairs created by the e-e Coulombic scattering processes and the effective e-ph vertex is largely suppressed in the small-momentum limit. This effect appears in a direct calculation of the expression (31) for the effective e-ph vertex in the presence of LRC forces, $\Lambda_{\text{LR}}^{e\text{-ph}}(k,q;\omega_m)$. Now $\mu,\nu=r,\lambda,Y$ in Eq. (31), so as to include the screening due to the fluctuations of the ''long-range'' boson Y. In particular Fig. 7 shows the momentum dependence of the static ($\omega_n=0$) e-ph vertex. The comparison with the same quantity in the absence of LRC forces shows a striking difference in the low-momentum region, where the Coulombic screening leads to a vanishing e-ph vertex. This difference can easily be understood by a three-step evaluation of $\Lambda_{\text{LR}}^{e\text{-ph}}(k,q;\omega_m)$. One can first go through the calculation of the vertex in the absence of LRC forces [Eq. (31)]. Then one can introduce a density-density fermionic bubble dressed by all electronic short-range processes,

$$\Pi^{e\text{SR}}(q,\omega_m)=\frac{4r_0^2P^0(q,\omega_m)}{\det D^{2\times2}(q,\omega_m)}, \tag{43}$$

where $D^{2\times2}$ is the 2×2 sector of the boson propagator only including the r and λ bosons, representing the purely electronic short-range processes. Finally one performs a resummation only including Y-boson fluctuations dressed by the $\Pi^{e\text{SR}}$ density-density fermionic bubbles. The result is

$$\Lambda_{\text{LR}}^{e\text{-ph}}(k,q;\omega_m)=\frac{\Lambda^{e\text{-ph}}(k,q;\omega_m)}{1+\Pi^{e\text{SR}}(q;\omega_m)V_C/[\sqrt{A^2(q)-1}]}. \tag{44}$$

This expression readily shows the suppression of the short-range-only e-ph vertex appearing in the numerator and clearly displays the vanishing of the LR vertex for $q\to0$, when the Coulombic potential diverges $[A^2(q)-1]^{-1}\to|\mathbf{q}|^{-1}$.

The important physical consequence of the above suppression of the effective e-ph vertex is that in the presence of LRC forces the long-wavelength density fluctuations are decoupled from the phonons and become unable to drive a low-momentum instability. Nevertheless, the possibility of finite-momentum instabilities still remains open and a detailed reanalysis of the phase diagram in the presence of the LRC potential is needed. This analysis can be carried out by direct numerical evaluation of the *static* density-density response function and of its divergences. A direct inspection to the diagrammatic structure of leading order in the $1/N$ density-density response function shows that one can include the Coulombic effects both by extending the μ,ν summations in Eq. (17) to include the Y boson or, alternatively, by first calculating the short-range response function P^{SR} by only including the r, λ, and a bosons and then to resum with the bare $\langle YY\rangle$ propagator. The result is then

$$P^{\text{LR}}(q,\omega=0)=\frac{P^{\text{SR}}(q,\omega=0)}{1+\{V_C/[N\sqrt{A^2(q)-1}]\}P^{\text{SR}}(q,\omega=0)}. \tag{45}$$

From this expression one can easily see that a positively diverging $P^{\text{SR}}(q,\omega=0)$ no longer gives a diverging LR density-density response function. In particular, since $V_C/[\sqrt{A^2(q)-1}]\to\infty$ for $q\to0$, the compressibility always vanishes as it should in a Coulomb gas and a PS instability is now ruled out. However, some finite-q instabilities are still possible in the system when

$$P^{\text{SR}}(q,\omega=0)=-N[\sqrt{A^2(q)-1}]/V_C, \tag{46}$$

leading to a divergent P^{LR}. This is possible, in principle, since inside the PS region for the model without LRC forces, P^{SR} has a simple pole. Therefore P^{SR} has a negative branch from zero momentum up to sizable momenta (if the parameters are choosen to be inside enough into the unstable region) and the condition (46) can be satisfied. At this point, then, an instability occurs despite the stabilizing effect of the LRC potential and an incommensurate charge-density-wave (CDW) phase takes place in the system.

The g vs δ phase diagram for various values of V_C is reported in Fig. 8, where the solid line represents the place at which $P^{\text{LR}}(q=q_c,\ \omega=0)$ diverges, separating the stable uniform region from the unstable region where an incommensurate CDW is expected to form. It is important to notice that, when the settling of a CDW phase is given by a second-order quantum transition, no Maxwell construction is needed to determine the stability region.

As can be seen the effect of LRC forces is stronger at low doping. This is so because in this region the poles of P^{SR} tend to occur at low momenta and are more effectively stabilized by the Coulombic potential.

We found that the momenta q_c at which the divergences in P^{LR} occur obviously depend on the point g vs δ and on the strength of the Coulomb force V_C, but are generically sizable, indicating that the wavelength of the expected CDW phase is of a few unit cells.

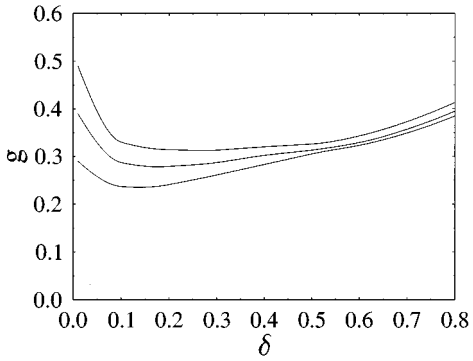

FIG. 8. Phase diagram e-ph coupling g vs doping δ with $t_{\mathrm{phys}}=0.5$ eV, $t'=-(1/6)t$, and $\omega_{0\,\mathrm{phys}}=0.04$ eV, and in the presence of LRC forces with $V_{C\mathrm{phys}}=0.55$ eV (lowest curve), $V_{C\mathrm{phys}}=1.65$ eV (middle curve), and $V_{C\mathrm{phys}}=3.3$ eV (upper curve).

We performed an extensive analysis of the finite-q instabilities for various values of doping, t'/t, g, and V_C. It turns out that, for reasonable values of these parameters, the instabilities always occur at or close to the (1,0) and (0,1) directions. This effect is due to the momentum structure of the short-range density-density response function, which is enhanced by the large density of states in the (1,0) and (0,1) directions.

It is interesting to notice that, close to the finite-q instability, the static effective scattering amplitude in the particle-hole as well as in the particle-particle channel diverges at finite momentum transfer like[9]

$$\Gamma(q,\omega=0)=\widetilde{U}-\frac{A}{D'+B'|\boldsymbol{q}-\boldsymbol{q}_c|^2}, \tag{47}$$

with $D'\propto(\delta-\delta_c)$ being a mass linearly vanishing by approaching δ_c. The evolution of $\Gamma(k_F,k_F',\omega=0)$ in approaching the unstable region by doping variations is displayed in Fig. 9. Figure 10 displays $\Gamma(k_F,k_F',\omega=0)$ over a large portion of the Brillouin zone for parameter values close

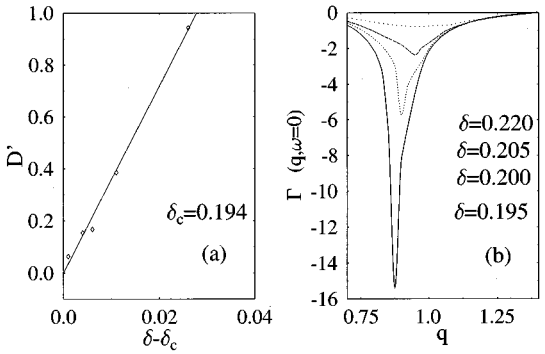

FIG. 9. (a) Mass D' of the effective static scattering amplitude as a function of $\delta-\delta_c$ for $t_{\mathrm{phys}}=0.5$ eV, $t'=-1/6t$, $V_{C\mathrm{phys}}=0.55$ eV, $\omega_{0\mathrm{phys}}=0.04$ eV, and $g_{\mathrm{phys}}=0.240/\sqrt{2}$ eV. The open squares indicate the values of D at various dopings and the straight line is a linear fit. (b) Static scattering amplitude for the same parameters as in (a) as a function of the transferred momentum $\boldsymbol{q}$ in the $\boldsymbol{q}_c\approx(\pm0.28/a,\pm0.86/a)$ direction. The doping $\delta=0.195$, 0.2, 0.205, and 0.22 increases from the lower solid line to the upper dotted line.

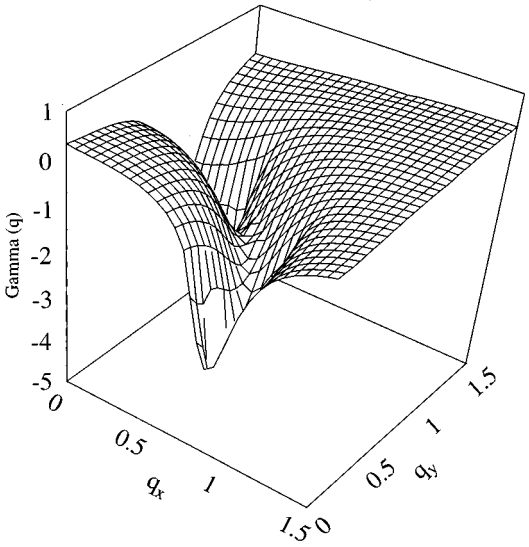

FIG. 10. Momentum dependence of the static scattering amplitude for the same parameters as in Fig. 9 at $\delta=0.195$.

to those of a finite-q instability. It is evident that a deep attractive interaction between the quasiparticles arises on a broad momentum region. This fact is particularly remarkable in relation to the occurrence of Cooper instabilities. As seen in Sec. III A, a static Cooper instability takes place when the Fermi-surface average of $-\Gamma^C(k_F,k_F',\omega=0)$ becomes positive [cf. Eq. (27)] and this seems likely to occur close to finite-momentum instabilities. The resulting coupling constants are reported in Table II. As expected, positive (i.e., attractive) coupling constants arise close to the incommensurate CDW instability, once more supporting the idea that high-temperature superconductivity could arise in the proximity of a charge instability. It is also worth emphasizing that, like in the proximity of PS, such a pairing instability takes place as an effect of a q-independent phonon-induced attraction, which, close to the CDW instability, becomes highly structured in momentum space, thereby opening the way to pairing symmetries other than the simple s wave. This fact accounts for the attractive couplings also found in the d-wave channel. In particular it turns out that the d-wave symmetry of the order parameter is able to take good advantage of the strong small-q attraction and of the local (large-q) repulsion.

In the region of small to intermediate g's and dopings our analysis indicates the sure existence of d-wave pairing in sizable regions near the instability, whereas the occurrence of s-wave pairing takes place in a much narrower region. However, it should be emphasized that the presence of a

TABLE II. Extended s- and d-wave superconducting couplings for $t_{\mathrm{phys}}=0.5$ eV, $t=-1/6t'$, $g_{\mathrm{phys}}=0.260/\sqrt{2}$ eV, $\omega_{0\mathrm{phys}}=0.04$ eV, and $V_{C\mathrm{phys}}=0.55$ eV at various dopings. The instability is at $\delta_c=0.299$.

δ	0.300	0.305	0.310	0.330	0.360	0.400
λ_{s_1}	0.134	0.076	0.048	−0.024		
λ_{d_1}	0.372	0.206	0.174	0.110	0.070	0.045

s-wave static Cooper instability only in a narrow region by no means excludes the possibility of having s-wave superconductivity in a much larger area of our phase diagram. An appropriate Eliashberg dynamical analysis would be required to draw a firm conclusion, especially in the light of the results reported in the next section showing a strong frequency dependence of the effective interaction between the quasiparticles. Of course the same applies to the attraction in the d-wave channels, which could also be greatly favored by dynamical effects.

C. Dynamical properties

We carried out a dynamical analysis of the effective e-ph vertex in the presence of LRC forces. The dynamical behavior of the e-ph vertex in the presence of LRC forces is not very different from the behavior observed for $V_C=0$. In both cases two different screening regimes take place for small and large momenta. Specifically, when LRC forces are absent, we found that at small momenta the screening energy $\omega_{\rm scr}$ is proportional to the doping and depends linearly on the exchanged momentum $\omega_{\rm scr}\approx v_F^* q$. Instead, in the presence of LRC forces, it is found that

$$\omega_{\rm scr}\approx\sqrt{v_F^* q}. \tag{48}$$

The linear momentum dependence in the short-range-only case is compatible with screening processes associated with both the particle-hole continuum and the zero sound. In the presence of LRC forces, the square-root momentum dependence is a clear indication that the plasmon collective mode[46] sets the cutoff energy at which small-momentum screening processes cease to be relevant.

On the other hand, we found that at large momenta, a different energy scale rules the screening processes, which, both with and without LRC forces, is of the order of the bare-electron hopping t, $\omega_{\rm scr}\approx\gamma t$. This indicates that the local (large-q) physics is governed by incoherent bare-electron processes with typical energies of order t much larger than the typical energies of order $v_F^* q\sim t\delta$ ruling the coherent quasiparticle processes.

The screening effects leading to different behaviors of the effective e-ph vertex at small and large momenta also affect the dynamical scattering amplitude. This generic effect is more evident in the proximity of an instability. Therefore, in Fig. 11, we show the numerical evaluation of the dynamical scattering amplitude. A large attraction at low frequency is found for transferred momenta close to q_c as a remnant of the infinite static attraction taking place at the instability. This attraction is, however, rapidly spoiled by increasing the Matsubara frequency. This is so because at finite $q\approx q_c$ the dynamical screening of the e-ph vertex strongly suppresses the phononic attractive part of the scattering amplitude. Therefore, as soon as the frequency spoils the static attraction due to the instability, the attractive part of Γ^C (dotted line in Fig. 11) rapidly vanishes. An opposite behavior occurs at small momenta, where no instability occurs and therefore no static attraction is present. The usual e-ph attraction only appears at a finite frequency around $\omega_0>\omega_{\rm scr}\approx q\delta$, where the e-ph vertex is not severely suppressed.

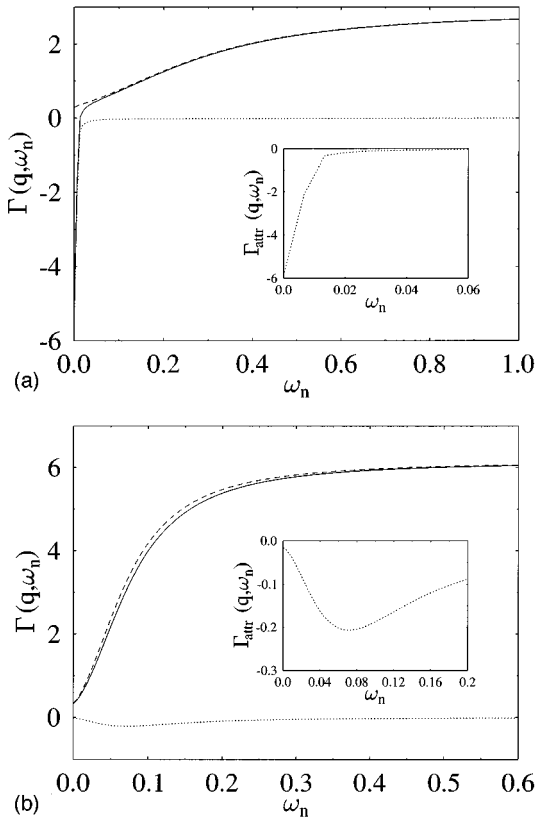

FIG. 11. Effective scattering amplitude as a function of the transferred Matsubara frequency for $t_{\rm phys}=0.5$ eV, $t'=-(1/6)t$, $g_{\rm phys}=0.240/\sqrt{2}$ eV, $\omega_{0\rm phys}=0.04$ eV, and $V_{C\rm phys}=0.55$ eV. The doping $\delta=0.2$ is close to the critical value $\delta_c=0.195$. Solid line, total effective scattering amplitude Γ; dashed line, repulsive (slave and Coulomb force bosons only) effective scattering amplitude $\Gamma_{\rm rep}$; dotted lines, attractive part of the scattering amplitude $\Gamma_{\rm attr}=\Gamma-\Gamma_{\rm rep}$. The transferred momenta are in the instability direction (0.28,0.86). (a) Sizable transferred momentum $|\boldsymbol{q}|=|\boldsymbol{q}_c|=0.9$; (b) small transferred momentum $|\boldsymbol{q}|=0.15$ The insets are enlargements of the attractive parts of the effective scattering amplitudes.

We conclude this subsection by recalling the result of Ref. 9 where a real-frequency analysis was carried out finding strong singular scattering between the quasiparticles of the form

$$\Gamma(\boldsymbol{q},\omega)\approx\widetilde{U}-\frac{A}{\omega_{\boldsymbol{q}}-i\omega}, \tag{49}$$

where $\omega_{\boldsymbol{q}}=D'+B'|\boldsymbol{q}-\boldsymbol{q}_c|^2$ with $D'\propto(\delta-\delta_c)$. This scattering is of the form proposed in Ref. 5 to explain the anomalous normal-state properties of the superconducting copper oxides. Some substantial differences are, however, worth being emphasized. First of all the origin of the singular behavior is not necessarily related to a magnetic scattering mechanism, in so far it arises from the closeness to a charge instability. The mechanism driving the instability can be of various nature, magnetic, excitonic, or, as in the present model, phononic. Second, as can be seen in Fig. 10, a much more isotropic region of large scattering arises in the present context, thereby bypassing the objection raised in Ref. 47 that only a few ''hot'' points on the Fermi surface undergo such strong scattering processes.

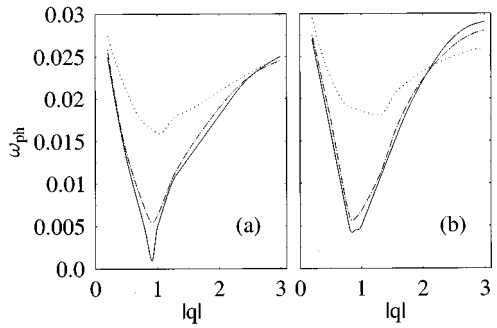

FIG. 12. Phonon dispersion curves (a) in the instability (0.28,0.86) direction and (b) in the (1,1) direction, for $t_{\mathrm{phys}}=0.5$ eV, $t'=-(1/6)t$, $g_{\mathrm{phys}}=0.240/\sqrt{2}$ eV, $\omega_{0\,\mathrm{phys}}=0.04$ eV, and $V_{C\mathrm{phys}}=0.55$ eV. The solid curves correspond to the critical doping $\delta_c=0.195$; the dot-dashed and dotted curves correspond to $\delta=0.21$ and $\delta=0.3$, respectively.

D. Collective modes

The analysis of the dynamical behavior of the model can be completed by investigating the collective modes present in the system. This study is particularly relevant for a deep understanding of the dynamical mechanisms ruling the instability formation. To emphasize similarities and differences we consider both the cases with and without the LRC potential.

It was repeatedly pointed out, in the context of models with short-range interactions only, that PS occurs without a softening of a massive collective mode. This was first established for the charge-transfer mode in a three-band Hubbard model with NN Coulombic repulsion between copper and oxygen holes[18] and it was also confirmed in the case of a three-band Hubbard-Holstein model with holes coupled to an optical phonon.[20] A real-frequency analysis of both the imaginary part of the dynamical density-density correlation function, $\mathrm{Im}\langle nn\rangle(q,\omega)$, and of the poles of the phonon propagator, $D^{a,a}(q,\omega)$, shows that also in the single-band infinite-U Hubbard-Holstein model, PS occurs due to the phonon-mediated attraction between quasiparticles, which pulls the zero-sound mode into the particle-hole continuum. When the attraction is large enough, the velocity of this strongly damped mode vanishes, eventually driving the system unstable at zero momentum. On the contrary, the phonon frequency, although sizably renormalized by the e-ph interaction, stays finite over the entire Brillouin zone.

The scenario is strongly modified in the presence of LRC forces, when the instability takes place at finite momenta. For such finite momenta, in the absence of e-ph interactions the phonon is the mode at lower energy. With the introduction of a finite e-ph coupling, it turns out that the phonon is somewhat softened. In particular the softening is complete, i.e., the phonon energy vanishes, when the CDW instability takes place. Again a comparative real-frequency analysis of $\mathrm{Im}\langle nn\rangle(q,\omega)$ and of $\mathrm{Im}D^{a,a}(q,\omega)$ allows us to identify the nature of the mode entering the continuum and producing the large enhancement of the absorption at low-frequency. Figure 12(a) reports the behavior of the phonon frequency [extracted from $\mathrm{Im}D^{44}(q,\omega)$] as a function of momenta in the specific direction at which the CDW instability takes place [$(\pm 0.2,\pm 0.8)$ and $(\pm 0.8,\pm 0.2)$ for the parameters related to 214 systems] at and above the critical doping value. In Fig. 12(b) the phonon dispersions are reported for the $(\pm 1,\pm 1)$ direction for the same values of doping. Far from the critical momentum the phonon frequency is sizably reduced with respect to its bare value. However, only a minor doping dependence of this substantial reduction is visible in generic positions in the Brillouin zone, making the observation of the softening effect rather difficult. On the other hand, a strong doping dependence of the phonon dispersion is apparent in the proximity of the critical momentum. In this momentum region the phonon completely softens at $\delta=\delta_c=0.195$. By increasing the doping, i.e., by moving away from the instability, the softening becomes incomplete and progressively less important although it seems to stay substantial up to $\delta=0.3$.

Some considerations are in order on the above analysis of the collective modes in the proximity of charge instabilitites. First of all a clear distinction can be made between the behavior of the phonon mode in the absence and in the presence of LRC forces. At a PS instability, the phonon always stays massive and only mixes strongly with a low-energy zero-sound mode at finite but very small momenta ($q\leqslant\omega_0/v_F^*$). On the contrary the phonon becomes completely soft at the CDW instability. Therefore it would be natural to indicate neutron-scattering experiments in copper oxides as crucial tests in order to determine how close these material are to a *phonon-mediated* CDW instability: If a substantial softening of some phonon mode is found at some momenta, this would be a clear indication of a frustrated PS almost leading to CDW. Unfortunately, our schematic single-band Hubbard-Holstein model is not detailed enough to provide indications of the modes which could undergo a visible softening in real materials. Moreover, the strong reduction of the phonon frequency is substantial on a sizable momentum range, but is only found for doping close to the critical δ_c, and this fact could render the search for such an effect quite a difficult task. An additional difficulty is that, due to the strong mixing of electronic and phononic degrees of freedom, the softened phonon modes would be greatly broadened and they could well be seen only as an increase of spectral weight at low frequencies, quite differently from the theoretical $1/N$ picture reported in Fig. 12.

V. DISCUSSION AND CONCLUSIONS

In this paper we analyzed the screening processes and the occurrence of instabilities in the Hubbard-Holstein model in the framework of Fermi-liquid theory. In particular we investigated the role of LRC forces in stabilizing PS and producing incommensurate CDW instabilities.

However, some limitations should be kept clear for a correct understanding of the scenario here presented. We carried out a leading order analysis in $1/N$, which definitely neglects some effects which are relevant in a complete quantitative understanding of the real materials. First of all our approach is designed to deal with charge degrees of freedom, but lacks a correct treatment of the spin degrees of freedom, which turn out to be crucial in the low-doping phase of the copper oxides. Therefore antiferromagnetic correlations and the interplay between spin and phonon degrees of freedom are absent in our large-N, slave-boson model. These effects only

appear at higher order in $1/N$. Second, our leading-order expansion does not allow for phonon vertex corrections beyond the Migdal theorem, although in the low-doping region the quasiparticle bands become very narrow, thus leading to a violation of the condition $E_F \gg \omega_0$. The absence of these vertex corrections obviously rules out the possibility of a correct observation of multiphonon polaronic effects.

In the absence of LRC forces, the scenario found here is consistent with previous results obtained in the three-band Hubbard-Holstein model, where PS was also found. The main features observed here are (i) a generic suppression of the e-ph vertex due to electronic screening also resulting in a strong dependence on the $v_F q/\omega$ ratio, (ii) the persistent possibility of PS arising from the phonon-mediated attraction, and (iii) a singular behavior of the effective interaction between quasiparticles at low momenta close to the PS region.

The main achievement of the present work is, however, the analysis of the model in the presence of LRC forces. In particular it is remarkable that, when LRC forces are included in the model, PS is spoiled, but finite-momentum instabilities still take place on substantial and quite physical regions of the parameter space. Singular effective interactions are again obtained at finite momenta in the proximity of the CDW instability. (iv) Cooper pairing both in the s- and the d-wave channels is present already in the static limit for systems close enough to the unstable regions, both in the presence and in the absence of LRC forces.

The present model provides a rather simple playground to investigate the generic properties of electronic systems close to charge instabilities. Indeed, while some properties like, e.g., the behavior of the phonon mode are strictly related to the phononic nature of the interaction here considered, the main results obtained here are generic of models[17] showing charge instabilities. In particular we believe that the strict relation between charge instabilities, strong scattering, and Cooper pair formation [points (iii) and (iv) above] is a generic feature of strongly correlated electron systems irrespective of the underlying physical mechanisms leading to PS or to incommensurate CDW.

Note added in proof: In relation to our results in Sec. IV D, we mention that indications of anomalous lattice behavior are indeed reported by Kohara *et al.* [Phys. Rev. Lett. **70**, 3447 (1993)], (we thank Professor V. J. Emery for indicating this reference to us) and L. Pintschovius *et al.* [Physica C **185–189**, 156 (1991)].

ACKNOWLEDGMENTS

The authors acknowledge interesting discussions with Professor C. Castellani. This work was also supported by the Istituto Nazionale per la Fisica della Materia.

APPENDIX: THE MAXWELL CONSTRUCTION

In order to perform the Maxwell construction, we modify the model in Eq. (1), coupling the phonons to the full electron density rather than to the density fluctuations. In this way an e-ph coupling is effective already at the mean-field level, where a nonzero mean-field value of the phonon field, $a_0 = \langle a \rangle = \langle a^\dagger \rangle$, arises. The mean-field Hamiltonian acquires the form

$$H'_{\mathrm{MF}} = \sum_{k\sigma} E_k c^\dagger_{k\sigma} c_{k\sigma} - (\mu_0 - \lambda_0 + 2g a_0) \sum_{k\sigma} c^\dagger_{k\sigma} c_{k\sigma} + N\lambda_0 \left(r_0^2 - \frac{1}{2} \right) + N\omega_0 a_0^2 . \tag{A1}$$

Minimizing the mean-field free energy with respect to a_0 allows us to obtain the self-consistency equation for a_0:

$$N\omega_0 a_0 = Ng \sum_k f(E(k)) = g \frac{N}{2} (1 - \delta). \tag{A2}$$

This determines the phonon-induced shift of the chemical potential, giving rise to a doping-dependent correction to this quantity. Owing to the standard expression for the compressibility $\kappa \equiv \partial n / \partial \mu = -\partial \delta / \partial \mu$, the $q = 0$ instability can be read directly from the μ vs n curves: A stationary point in $\mu(\delta)$ corresponds to an infinite compressibility and a standard Maxwell construction in $\mu(\delta)$ determines the region where the system is in a single phase.

[1] For a review on experiments in high-temperature superconductors see, e.g., Proceedings of the International Conference on Materials and Mechanisms of Superconductivity High Temperature Superconductors, Grenoble, France, 1994 [Physica C **235-240** (1994)].

[2] P. W. Anderson, Science **235**, 1196 (1987); Phys. Rev. Lett. **64**, 1839 (1990); **65**, 2306 (1990).

[3] For a review see *The Physics and the Mathematical Physics of the Hubbard Model*, edited by D. Campbell (Plenum Press, New York, 1995).

[4] C. Castellani, C. Di Castro, and W. Metzner, Phys. Rev. Lett. **72**, 316 (1994).

[5] P. Montoux and D. Pines, Phys. Rev. B **50**, 16 015 (1994).

[6] C. M. Varma, Int. J. Mod. Phys. B **3**, 2083 (1989).

[7] N. Nagaosa and P. A. Lee, Phys. Rev. Lett. **64**, 2450 (1990); P. A. Lee and N. Nagaosa, Phys. Rev. B **46**, 5621 (1992).

[8] V. J. Emery and S. A. Kivelson, in *Phase Separation in Cuprate Superconductors* (Ref. 10); V. J. Emery and S. A. Kivelson, Physica C **209**, 597 (1993); U. Löw, V. J. Emery, K. Fabricius, and S. A. Kivelson, Phys. Rev. Lett. **72**, 1918 (1994).

[9] C. Castellani, C. Di Castro, and M. Grilli, Phys. Rev. Lett. **75**, 4650 (1995).

[10] For a general review on phase separation in superconducting copper oxides see, e.g., *Phase Separation in Cuprate Superconductors*, edited by K. A. Müller and G. Benedek (World Scientific, Singapore, 1992); *Phase Separation in Cuprate Superconductors*, edited by K. A. Müller and E. Sigmund (Springer-Verlag, Berlin, 1994).

[11] C. Di Castro and M. Grilli, Phys. Scr. **T45**, 81 (1992).

[12] M. Marder, N. Papanicolau, and G. C. Psaltakis Phys. Rev. B **41**, 6920 (1990).

[13] V. J. Emery, S. A. Kivelson, and H. Q. Lin, Phys. Rev. Lett. **64**, 475 (1990).

[14] E. Dagotto, A. Moreo, F. Ortolani, D. Poilblanc, and J. Riera,

Phys. Rev. B **45**, 10 741 (1992).
[15] C. Castellani, M. Grilli, and G. Kotliar, Phys. Rev. B **43**, 8000 (1991); S. Caprara and M. Grilli, *ibid.* **49**, 697 (1994).
[16] N. Cancrini, S. Caprara, C. Castellani, C. Di Castro, M. Grilli, and R. Raimondi, Europhys. Lett. **14**, 597 (1991).
[17] M. Grilli, R. Raimondi, C. Castellani, C. Di Castro, and G. Kotliar, Phys. Rev. Lett. **67**, 259 (1991).
[18] R. Raimondi, C. Castellani, M. Grilli, Y. Bang, and G. Kotliar, Phys. Rev. B **47**, 3331 (1993).
[19] S. Caprara, C. Di Castro, and M. Grilli, Phys. Rev. B **51**, 9286 (1995).
[20] M. Grilli and C. Castellani, Phys. Rev. B **50**, 16 880 (1994).
[21] This second possibility was suggested for a different model in Ref. 18 together with the alternative possibility of bubble formation of hole-rich and hole-poor phases.
[22] J. M. Tranquada, B. J. Sternlieb, J. D. Axe, Y. Nakamura, and S. Uchida, Nature **375**, 561 (1995).
[23] A. Bianconi, in Ref. 1 and references therein.
[24] J. Mesot, P. Allenspach, U. Staub, A. Furrer, and H. Mutka, Phys. Rev. Lett. **70**, 865 (1993).
[25] This possibility is also briefly discussed in J. Tranquada, in Proceedings of the Second International Workshop on Low-Energy Electrodynamics in Solids, Tr̂eŝt (Czech Republic), 1995 [Ferroelectrics (to be published)].
[26] See, e.g., *Lattice Effects in High Temperature Superconductors*, edited by Y. Bar-Yam, T. Egami, J. Mustre-de Leon, and A. R. Bishop (World Scientific, Singapore, 1992).
[27] J. P. Falck *et al.*, Phys. Rev. Lett. **69**, 1109 (1992); P. Calvani, M. Capizzi, S. Lupi, and G. Balestrino, Europhys. Lett. **31**, 473 (1995) and references therein; P. Calvani, M. Capizzi, S. Lupi, P. Maselli, A. Paolone, and P. Roy, Phys. Rev. B **53**, 2756 (1996).
[28] T. Holstein, Ann. Phys. (N.Y.) **8**, 325 (1959).
[29] S. E. Barnes, J. Phys. F **6**, 1375 (1976).
[30] P. Coleman, Phys. Rev. B **29**, 3035 (1984).
[31] N. Read and D. M. Newns, J. Phys. C **16**, 3273 (1983); N. Read, *ibid.* **18**, 2651 (1985).
[32] G. Kotliar and J. Liu, Phys. Rev. Lett. **61**, 1784 (1988).
[33] A. J. Millis and P. A. Lee, Phys. Rev. B **35**, 3394 (1987); G. Kotliar and A. R. Ruckenstein, Phys. Rev. Lett. **57**, 1362 (1986).
[34] A different possible approach is also viable, where the phonons are coupled with the density and not with its fluctuations only. Then the ion equilibrium positions must be determined self-consistently together with the other mean-field parameters as a function of doping and of the tight-binding parameters. In this latter scheme the effect of phonons is already present at mean-field level and plays a role in the behavior of the chemical potential as a function of filling. Therefore this scheme is needed in order to apply the Maxwell construction to determine the phase-separation region. The approach described in the text assumes instead that the mean-field effect of phonons is included in the bare tight-binding parameters. Despite this seeming difference, we checked that the two approaches give the same results (see Sec. III).
[35] It should be noted that the quasiparticle-boson vertices [Eqs. (9)–(11)] are constant or only depend on the incoming fermionic momenta via expressions proportional to the energy. As a result the quasiparticle on the Fermi surface only couples to the bosons via constant vertices $\Lambda_r=-4tr_0^2\varepsilon_{k_F}$, $\Lambda_\lambda=i$, and $\Lambda_a=-2g$, irrespective on their momenta.
[36] See, e.g., P. Nozières, *Theory of Interacting Fermi Systems* (Benjamin, New York, 1964).
[37] ε_{k_F} vanishes when $\alpha=t'/t=0$ and $\delta\to 0$. This effect simply arises from the specific form of the Fermi surfaces in the single-band Hubbard model with NN hopping only, where the constant-energy surfaces are determined by the condition $\cos(k_{xF})+\cos(k_{yF})=$const.. Then, at $\delta=0$, the Fermi energy reduces to a square where the constant is zero. Therefore, when the next-NN hopping integral t' is zero, one finds that, for any finite e-ph coupling g, the attractive part will dominate. At the same time the quasiparticle density of states diverges ($\nu^*\approx 1/\delta$) so that a very large and negative F_0^s arises. This shows that, at least within our large-N scheme, a phase-separation instability is always obtained for any finite g when the doping is small enough and $t'=0$. This is no longer true when a finite next-NN hopping integral t' is considered, which modifies the shape of the Fermi surface and leads to nonzero values for ε_{k_F} at zero doping.
[38] T. Tanamoto *et al.*, J. Phys. Soc. Jpn. **62**, 717 (1993).
[39] In our analysis we also established that ε_{k_F} is always positive for negative values of α (i.e., NN and next-NN hoppings opposite in sign), so that an additional attractive interaction besides the local Hubbard repulsion is needed to drive the system unstable. On the other hand, ε_{k_F} can be negative for low doping values when t and t' have the same sign, so that an instability can in principle occur even in the absence of a phononic attractive term λ_g in Γ_ω [R. Zeyher (private communication)]. We stress, however, that positive values of t' are unlikely to be relevant for the real copper oxides insofar they give rise to unrealistic shapes of the Fermi surface.
[40] On the other hand, it turns out that for unrealistically large doping the instability first takes place at sizable finite momenta (dashed line), leading to the formation of incommensurate charge-density waves (CDW's). In particular we found that the finite-momentum instability first takes place for momenta in the $(\pm 1,0)$ and $(0,\pm 1)$ directions and momenta $q=2k_F$ connecting regions with slightly larger density of states.
[41] Attractive superconducting couplings are also found both in the s-wave and d-wave channels in the region where the instability takes place at finite momenta.
[42] This possibility was shown within a mean-field treatment of the Kondo lattice model in Ref. 16.
[43] M. Kulić and R. Zeyher, Phys. Rev. B **49**, 4395 (1994).
[44] R. Zeyher and M. L. Kulić, Phys. Rev. B **54**, 8985 (1996).
[45] In Ref. 43, however, only the case with $\alpha=t'/t=0$ was considered, which is rather peculiar. This can be seen by considering again the small-q case of Eq. (29) for $t'=0$. In this particular case the effect of the static vertex at low doping is much less dramatic since this vertex is proportional to $[1+4tN\nu^*\varepsilon_{k_F}(\alpha=0)]^{-1}$, where $\varepsilon_{k_F}(\alpha=0)=[\cos(k_{Fx})+\cos(k_{Fy})]$ vanishes when $\delta\to 0$. This peculiarity of the single-band Hubbard model is not present once next-NN hopping terms are considered. In this latter case ε_{k_F} no longer vanishes at half-filling and the presence of a large quasiparticle density of states ν^* in the denominator leads to a large suppression of the e-ph interaction.
[46] It should be remembered that in two-dimensional systems embedded in a three-dimensional space, the plasma modes have a square-root momentum dependence, at least at small momenta.
[47] R. Hlubina and T. M. Rice, Phys. Rev. B **51**, 9253 (1995).